Article

SOURCE DATA | TRANSPARENT PROCESS

EMBO reports

Reduced hnRNPA3 increases *C9orf72* repeat RNA levels and dipeptide-repeat protein deposition

Kohji Mori[1,**,†], Yoshihiro Nihei[1], Thomas Arzberger[2,3,4], Qihui Zhou[2], Ian R Mackenzie[5], Andreas Hermann[6,7], Frank Hanisch[8,9], German Consortium for Frontotemporal Lobar Degeneration[‡], Bavarian Brain Banking Alliance[§], Frits Kamp[1], Brigitte Nuscher[1], Denise Orozco[2], Dieter Edbauer[2,10] & Christian Haass[1,2,10,*]

Abstract

Intronic hexanucleotide (G_4C_2) repeat expansions in *C9orf72* are genetically associated with frontotemporal lobar degeneration (FTLD) and amyotrophic lateral sclerosis (ALS). The repeat RNA accumulates within RNA foci but is also translated into disease characterizing dipeptide repeat proteins (DPR). Repeat-dependent toxicity may affect nuclear import. hnRNPA3 is a heterogeneous nuclear ribonucleoprotein, which specifically binds to the G_4C_2 repeat RNA. We now report that a reduction of nuclear hnRNPA3 leads to an increase of the repeat RNA as well as DPR production and deposition in primary neurons and a novel tissue culture model that reproduces features of the *C9orf72* pathology. In fibroblasts derived from patients carrying extended *C9orf72* repeats, nuclear RNA foci accumulated upon reduction of hnRNPA3. Neurons in the hippocampus of *C9orf72* patients are frequently devoid of hnRNPA3. Reduced nuclear hnRNPA3 in the hippocampus of patients with extended *C9orf72* repeats correlates with increased DPR deposition. Thus, reduced hnRNPA3 expression in *C9orf72* cases leads to increased levels of the repeat RNA as well as enhanced production and deposition of DPR proteins and RNA foci.

Keywords C9orf72; dipeptide repeat proteins; frontotemporal lobar degeneration; hnRNPA3; neurodegeneration

Subject Categories Molecular Biology of Disease; Neuroscience; RNA Biology

DOI 10.15252/embr.201541724 | Received 10 November 2015 | Revised 18 May 2016 | Accepted 30 June 2016 | Published online 26 July 2016

EMBO Reports (2016) 17: 1314–1325

Introduction

Unusual translation of bi-directionally transcribed intronic hexanucleotide repeats in the absence of ATG initiation codons in all reading frames leads to the generation of five distinct dipeptide repeat proteins (DPR), namely poly-GA, poly-GP, poly-GR, poly-AP, and poly-PR [1–5]. DPR accumulate in disease characterizing p62-positive and TDP-43-negative inclusions [1–4]. The G_4C_2 repeat RNA may trap RNA binding proteins and thus inhibit their normal function [6–8]. Indeed, we recently identified a number of G_4C_2 repeat binding proteins including hnRNPA1, A2 and A3 [6]. Strikingly, mutations in hnRNPA1 and A2 cause multisystem proteinopathy and the sites of the pathogenic mutations are conserved in hnRNPA3 [9]. Moreover, hnRNPA3 accumulates in a subset of p62-positive inclusions and may be reduced within hippocampal neurons of *C9orf72* mutation carriers [6]. We therefore investigated if a loss of hnRNPA3 may modulate DPR production and deposition.

1 Biomedical Center (BMC), Ludwig-Maximilians-University Munich, Munich, Germany
2 German Center for Neurodegenerative Diseases (DZNE), Munich, Germany
3 Center for Neuopathology and Prion Research, Ludwig-Maximilians-University Munich, Munich, Germany
4 Department of Psychiatry and Psychotherapy, Ludwig-Maximilians-University Munich, Munich, Germany
5 Department of Pathology, University of British Columbia and Vancouver General Hospital, Vancouver, Canada
6 Deptartment of Neurology and Center for Regenerative Therapies Dresden (CRTD), Technical University Dresden, Dresden, Germany
7 German Center for Neurodegenerative Diseases (DZNE), Dresden, Germany
8 Department of Neurology, Martin-Luther-University Halle-Wittenberg, Halle (Saale), Germany
9 Department of Neurology, Vivantes Humboldt-Klinikum, Berlin, Germany
10 Munich Cluster for System Neurology (SyNergy), Munich, Germany
*Corresponding author. Tel: +49 89 4400 46549; E-mail: christian.haass@mail03.med.uni-muenchen.de
**Corresponding author. Tel: +81 6 6879 3051; E-mail: kmori@psy.med.osaka-u.ac.jp
‡For the German Consortium for Frontotemporal Lobar Degeneration: Adrian Danek, Janine Diehl-Schmid, Klaus Fassbender, Hans Förstl, Johannes Kornhuber and Markus Otto
§For the Bavarian Brain Banking Alliance: Andres Ceballos-Baumann, Marianne Dieterich, Regina Feuerecker, Armin Giese, Hans Klünemann, Alexander Kurz, Johannes Levin, Stefan Lorenzl, Thomas Meyer, Georg Nübling, Sigrun Roeber and Adrian Danek
†Present address: Department of Psychiatry, Osaka University Graduate School of Medicine, Suita, Osaka, Japan

Results

hnRNPA3 modulates repeat RNA and poly-GA levels

Knockdown of hnRNPA3 but not of hnRNPA1, hnRNPA2 and hnRNPH significantly enhanced generation of poly-GA in HeLa cells expressing 80 G_4C_2 repeats under the EF1 promotor (Fig 1A and B), whereas overexpression of hnRNPA3 decreased poly-GA generation (Fig 1C and D). RT–qPCR analysis revealed a corresponding increase of G_4C_2 repeat RNA upon hnRNPA3 knockdown (Fig 1E). Consistent with this finding, more cells harboring repeat RNA foci were detected (Fig 1F and G).

hnRNPA3-mediated repression of G_4C_2 repeat RNA and poly-GA protein is dependent on its ability to bind RNA. Whereas ectopic hnRNPA3WT rescued repression of repeat RNA and poly-GA upon knockdown of endogenous hnRNPA3 (Figs 2A–C and EV1A and B), a mutant variant, which is unable to bind RNA [10], failed to do so (Fig 2A–C). Nuclear import of hnRNPA3 also appears to be required since an hnRNPA3 variant lacking a M9 nuclear localization signal (NLS) (mCh-A3ΔM9) fails to fully rescue repression of repeat RNA and poly-GA protein (Fig 2D–F). The remaining activity is likely due to M9-NLS independent residual nuclear import of hnRNPA3 (Fig EV1C). Although knockdown of hnRNPA2 fails to increase GA production (Fig 1A and B), hnRNPA2 overexpression restored repression of repeat RNA and poly-GA (Fig 2B and C). In line with this finding, knockdown of hnRNPA3 together with hnRNPA1 or hnRNPA2 further increased poly-GA expression suggesting that hnRNPA1 and hnRNPA2 can partially compensate hnRNPA3 function (Fig EV1D and E). Overall, these findings suggest that hnRNPA3 negatively regulates repeat RNA expression levels, a process, which requires the RNA binding capacity of hnRNPA3 as well as its nuclear import via the M9-NLS.

Reduction of hnRNPA3 leads to enhanced poly-GA, poly-GP, and poly-GR production in HeLa cells and primary hippocampal neurons

In the above experiments, we only detected the most efficiently translated GA protein [4]. To investigate whether production of the other DPRs is also increased by reduced hnRNPA3 expression, we thought to achieve higher repeat RNA levels by expressing 80 G_4C_2 repeats under the control of the strong CMV promotor (Fig EV2A and B). This indeed allowed detection of poly-GA, poly-GP, and poly-GR in Western blots (Fig EV2C) and by immunocytochemistry

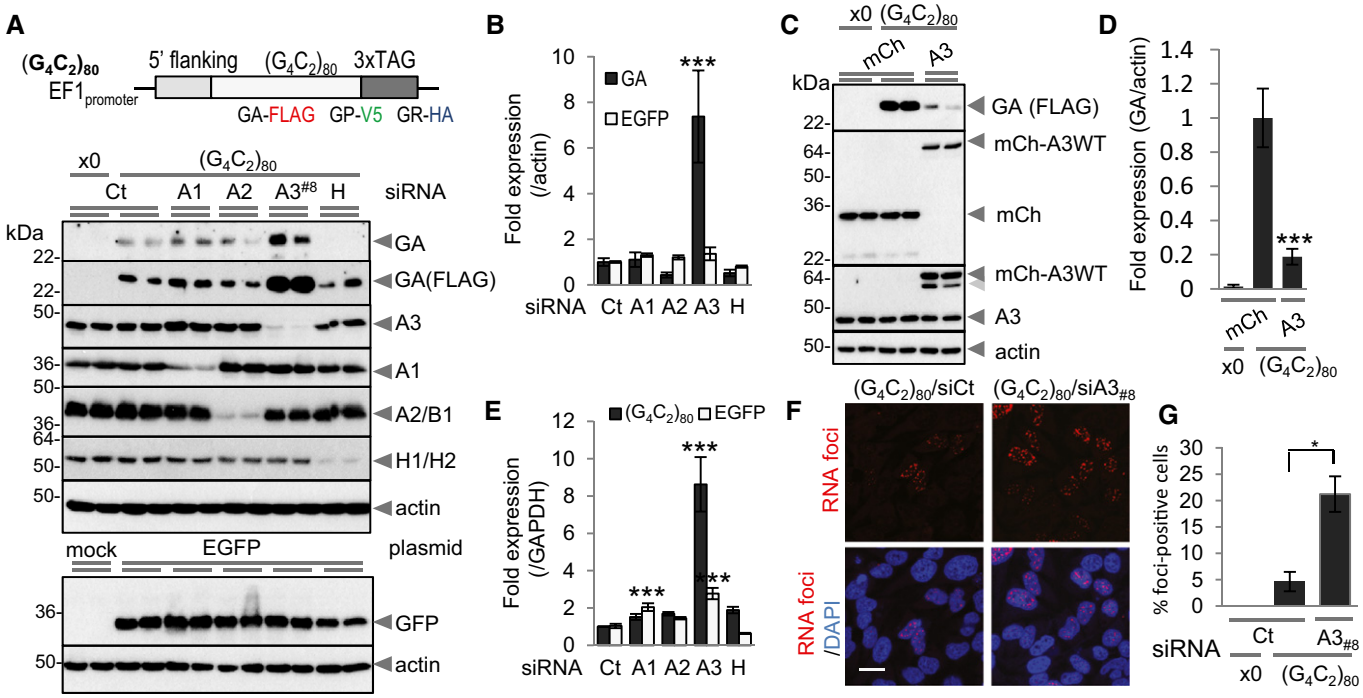

Figure 1. hnRNPA3 modulates repeat RNA and poly-GA expression.

A, B Knockdown of hnRNPA3 increases poly-GA expression, while expressions of EGFP protein levels are not altered upon knockdown of hnRNPs. The control ("x0") vector lacks the G_4C_2 repeats but still contains the 5′ flanking region and 3x TAG.

C, D Overexpression of hnRNPA3 suppresses poly-GA expression. n = 2 experiments performed in duplicates.

E Increased repeat RNA upon hnRNPA3 knockdown. EGFP RNA levels are only slightly increased as compared to the levels of the repeat RNA. n = 2 experiments performed in duplicates.

F, G Knockdown of hnRNPA3 increases RNA foci. n = 3 replicates; two-tailed paired t-test, Scale bar, 20 μm.

Data information: All graphs are shown as mean ± SEM. *P < 0.05, **P < 0.01, ***P < 0.001; two-tailed paired t-test (G), ANOVA with Dunnett's post-test (B, E) or ANOVA with Tukey's post-test (D).

Source data are available online for this figure.

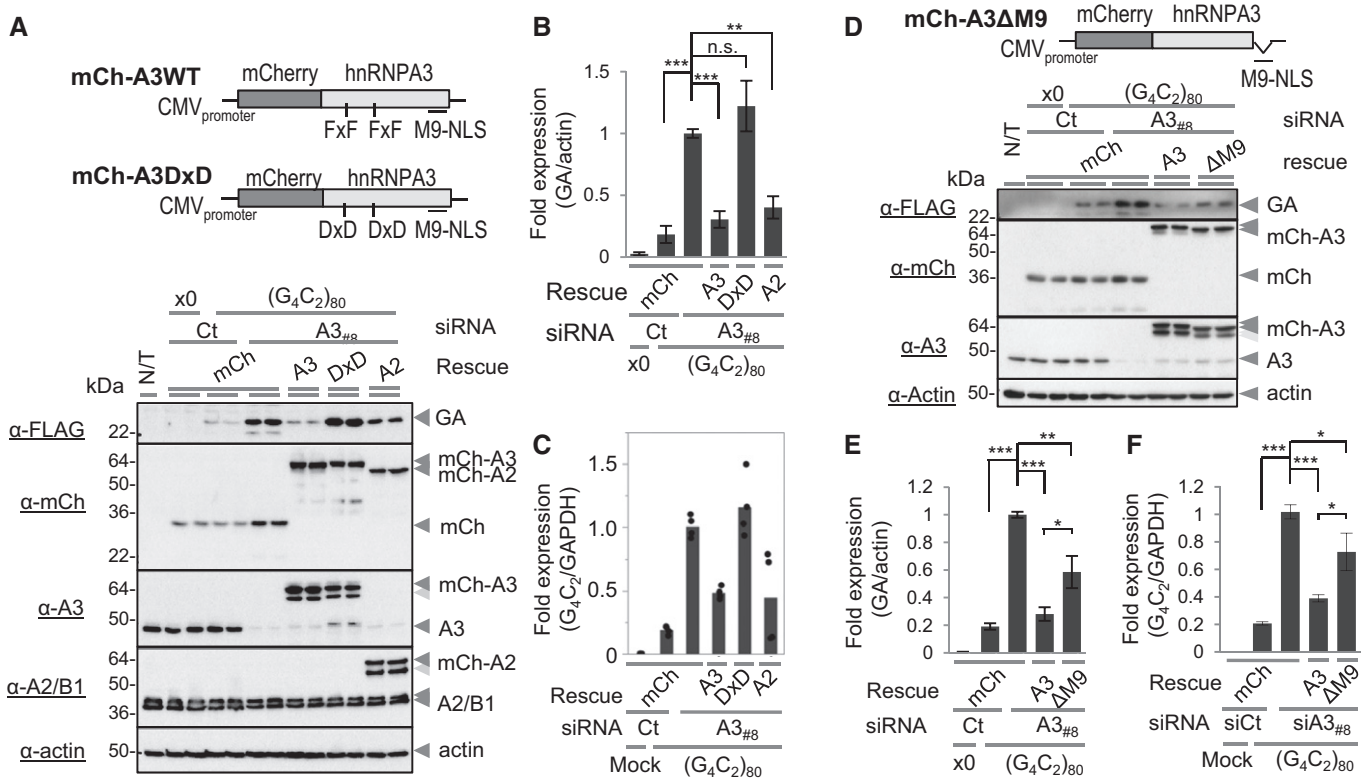

Figure 2. RNA binding and nuclear transport are required for hnRNPA3-mediated repression of poly-GA production.

A–C Rescue of repression of poly-GA and repeat RNA by wild-type (wt) hnRNPA3 and hnRNPA2 but not by the RNA binding mutant hnRNPA3DxD. (B) $n = 3$ experiments performed in duplicates; (C) $n = 2$ experiments performed in duplicates.

D–F Rescue of repression of poly-GA and repeat RNA by hnRNPA3WT but not the M9-NLS deletion mutant. (E) $n = 3$ experiments performed in duplicates; (F) $n = 4$ experiments performed in duplicates.

Data information: All graphs are shown as mean ± SEM. $^*P < 0.05$, $^{**}P < 0.01$, $^{***}P < 0.001$ ANOVA with Tukey's post-test. See also Fig EV1.

Source data are available online for this figure.

(Fig EV2D and E). Moreover, we detected p62-positive poly-GA deposits in a subset of cells (Fig 3A). Furthermore, poly-GA and poly-GR double-positive cells, but not poly-GA single-positive cells, frequently showed altered TDP-43 intracellular distribution (Figs 3B and EV3A and B) thus reproducing important pathological features of *C9orf72*-associated neuropathology. TDP-43 redistribution was typically associated with altered nuclear morphology, which may indicate onset of apoptosis. TDP-43 mislocalization was enhanced in cells, which express both, poly-GA and poly-GR (Figs 3B and EV3A and B). In line with the data shown in Fig 1, hnRNPA3 knockdown significantly increased $(G_4C_2)_{80}$ repeat RNA (Fig 3C) as well as poly-GA, poly-GP, and poly-GR protein with poly-GA being the most abundant DPR protein as observed in *C9orf72* patients [4] (Fig 3D–F). Furthermore, co-expression of two or three different DPRs in one cell was significantly more frequently detected in hnRNPA3-depleted cells (Fig 3G).

Similar findings were made in primary rat hippocampal neurons. shRNA knockdown of hnRNPA3 led to an increased accumulation of poly-GA-positive punctae in $(G_4C_2)_{80}$ expressing cells indicating enhanced DPR aggregation and deposition (Fig 4A and B). Indeed, filter trap analysis confirmed the enhanced accumulation of insoluble poly-GA aggregates upon reduction of hnRNPA3 (Fig 4C and D).

Figure 3. DPR expression and deposition.

A Poly-GA aggregates co-localize with p62-positive deposits.

B Redistribution of nuclear TDP-43 to the cytoplasm in a poly-GA/poly-GR double-positive cell. Note that nuclei of poly-GA/poly-GR double-positive cells are frequently disrupted.

C Knockdown of hnRNPA3 increases repeat RNA expression. $n = 2$ experiments performed in duplicates.

D Filter trap assay probed with anti-FLAG, anti-myc, or anti-HA antibodies reveal abundant DPR production.

E Relative expression level of poly-GA, poly-GP, and poly-GR normalized to GR. $n = 3$ experiments.

F Expression of all three DPRs is increased upon knockdown of hnRNPA3. Signals from knockdown with $siRNA_{\#8}$ were normalized to 1. $n = 3$ experiments.

G Co-expression of two/three different DPRs in single cells is increased upon hnRNPA3 knockdown. $n = 3$ replicates.

Data information: All graphs are shown as mean ± SEM. $^*P < 0.05$, $^{**}P < 0.01$, $^{***}P < 0.001$; two-tailed paired *t*-test (G), ANOVA with Dunnett's post-test (C, F, G) or ANOVA with Tukey's post-test (E). Scale bars, 20 μm. See also Figs EV2 and EV3.

Reduction of hnRNPA3 leads to enhanced formation of nuclear RNA foci in fibroblasts derived from patients with *C9orf72* repeat extensions

To test whether reduced hnRNPA3 also leads to enhanced *C9orf72*-associated phenotypes under physiological condition without ectopic expression of *C9orf72* repeat extensions, we used fibroblast lines derived from three independent and unrelated patients with confirmed *C9orf72* repeat extensions (Fig 5A; see also Materials and Methods for further clinical characterization). Since we could not detect DPR expression in primary patient-derived cells including neurons derived from induced pluripotent stem cells using several

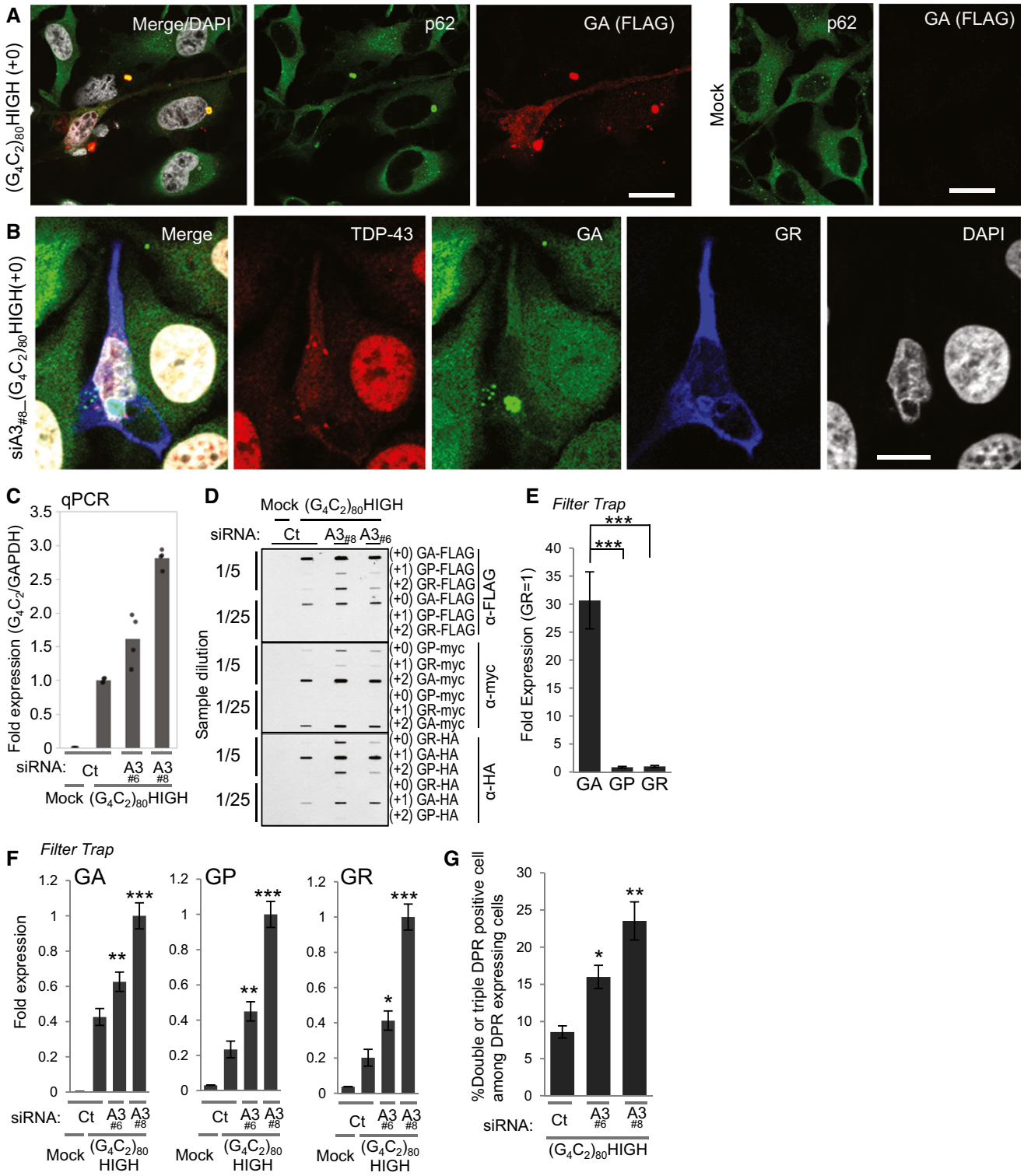

Figure 3.

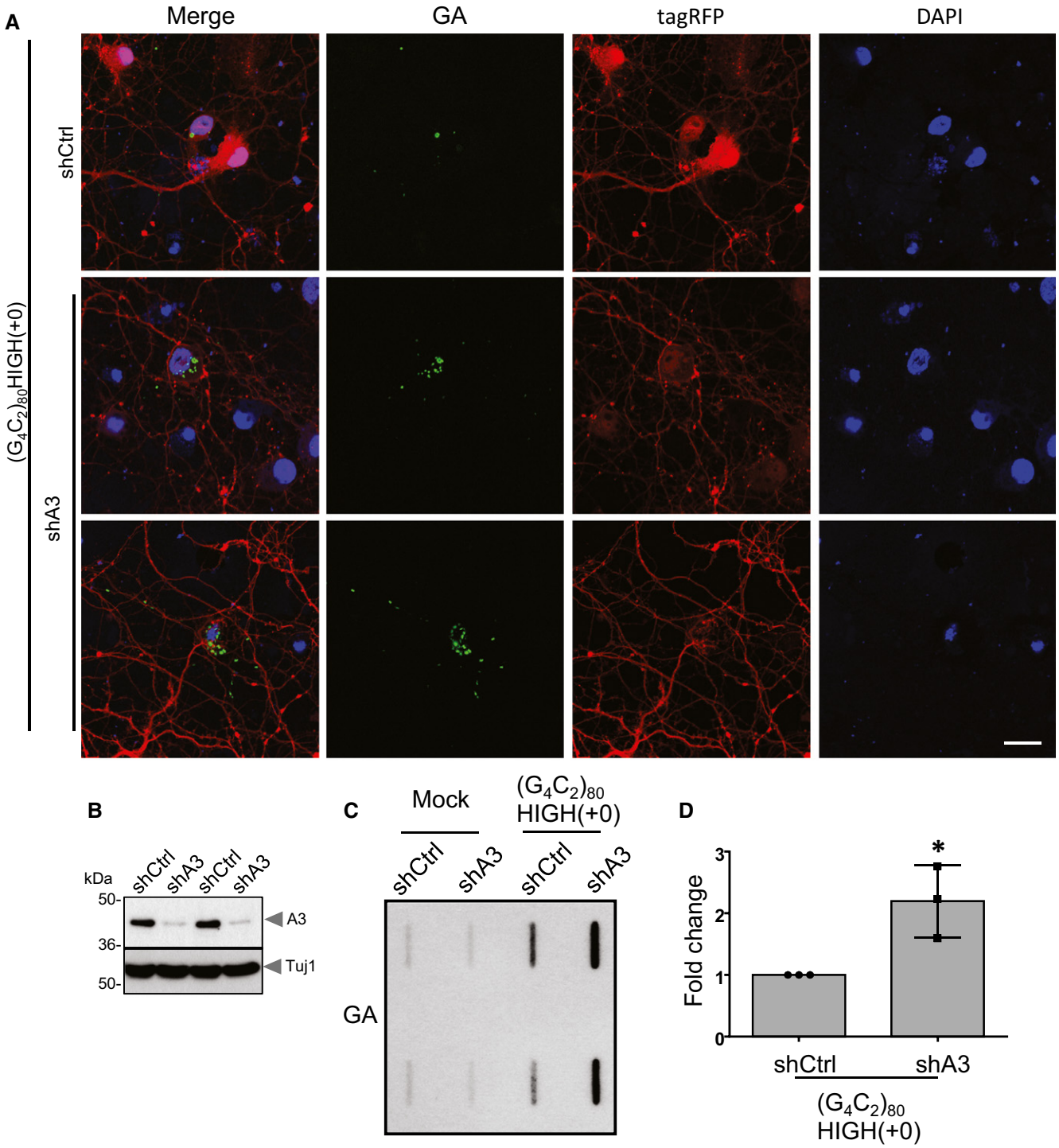

Figure 4. Knockdown of hnRNPA3 induces neuronal DPR accumulation.

Rat hippocampal neurons at DIV3 were transduced with lentivirus coexpressing either hnRNPA3 targeting shRNA (shA3) or a control shRNA (shCtrl) and tagRFP. Three days after transduction (DIV3 + 3), neurons were transfected with $(G_4C_2)_{80}$HIGH(+0) and analyzed at (DIV3 + 7).

A Neurons were fixed, immunostained, and imaged by confocal microscopy. Double immunofluorescence for poly-GA aggregates (green) and tagRFP (red). Nuclei were labeled with DAPI. Scale bar represents 20 μm.

B Efficient knockdown of endogenous rat hnRNPA3 with its targeting shRNA.

C Poly-GA aggregates were detected in a filter trap assay using an anti-Flag antibody.

D The amounts of poly-GA aggregates were quantified and are presented as the fold change of signals from neurons treated with the control shRNA or the repeat construct. Means ± SD of three independent experiments are shown. *$P < 0.05$ by a Student's *t*-test. $n = 3$ replicates.

Source data are available online for this figure.

A

Case	Sex	Age at disease onset (years old)	Age at biopsy (years old)	Disease duration (months)	Clinical phenotype
1	female	66	68	26	ALS, bulbar
2	female	49	51	36	ALS-FTD, bulbar
3	male	54	56	13	ALS, Spinal

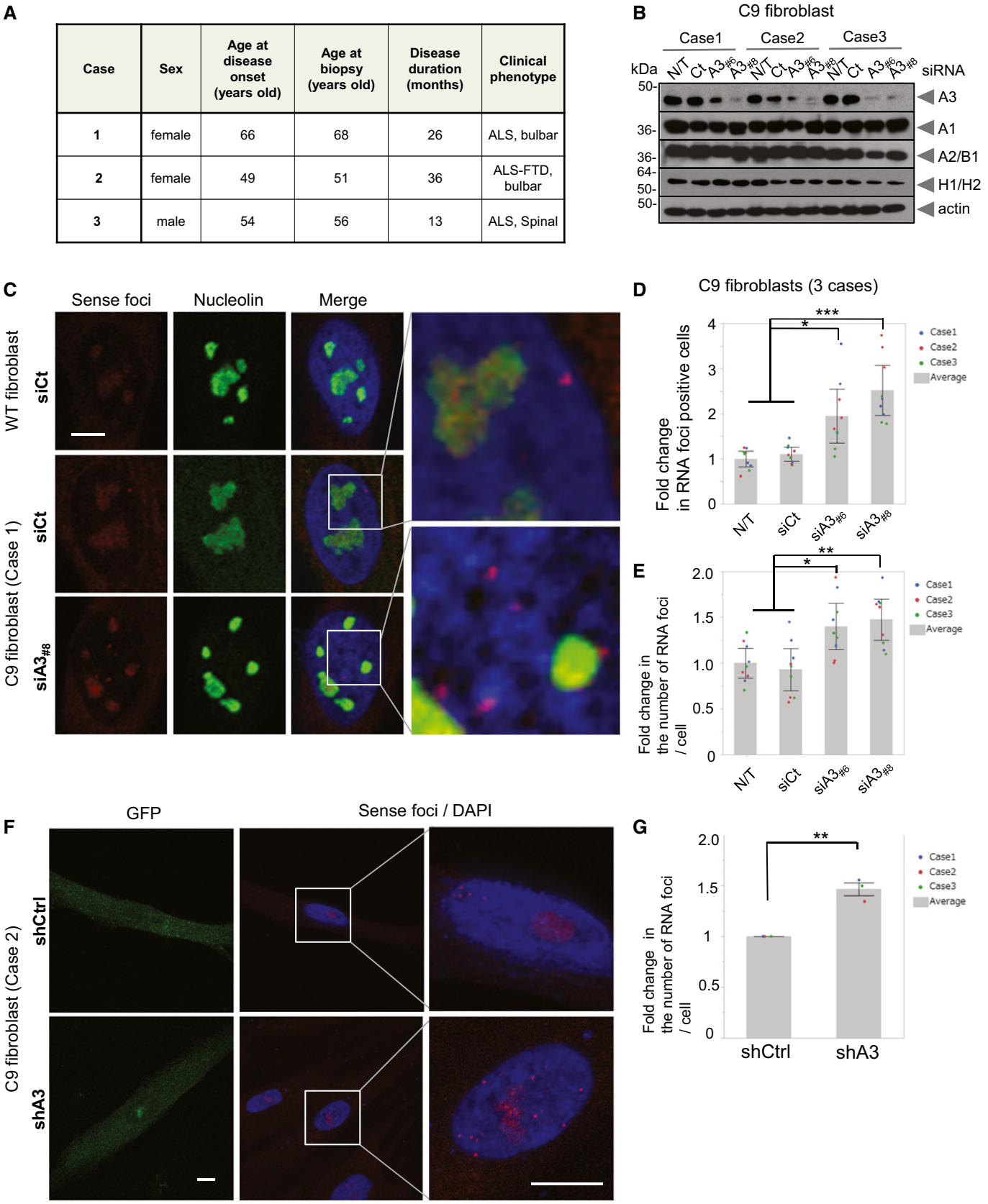

Figure 5.

Figure 5. Reduction of hnRNPA3 leads to enhanced formation of nuclear RNA foci in fibroblasts derived from patients with *C9orf72* repeat extensions.

A Fibroblasts from three individual patients with confirmed *C9orf72* repeat expansions were investigated.

B Knockdown of hnRNPA3 with two independent siRNA results in selective depletion of hnRNPA3 in fibroblasts from 3 *C9orf72* repeat carriers. Actin was used as a loading control.

C Knockdown of hnRNPA3 increases RNA foci in cells derived from *C9orf72* carriers. No G_4C_2 repeat RNA foci are detected in fibroblasts without *C9orf72* repeat expansions (WT). Nucleoli were stained with anti-nucleolin antibodies (green), and nuclei were stained with DAPI (blue). Scale bar, 10 μm.

D Quantification of the relative frequency of RNA foci-positive cells (RNA foci positivity; fold change). $n = 3$ experiments for each case. The average foci number of non-treated (N/T) fibroblast was normalized to 1. Color code labels values obtained in fibroblasts derived from the three individual patients. Bars indicate mean, individual points indicate mean values obtained from a single experiment (49–214 cells were counted in a single experiment), and error bars indicate 95% CI. $^*P < 0.05$, $^{***}P < 0.001$; ANOVA with Tukey–Kramer HSD test.

E Quantification of the number of RNA foci per RNA foci-positive cell (fold change). $n = 3$ experiments for each case. The average foci number of non-treated (N/T) fibroblast was normalized to 1. Color code labels values obtained in fibroblasts derived from the three individual patients. Bars indicate mean, individual points indicate mean values obtained from a single experiment (49–214 cells were counted in a single experiment), and error bars indicate 95% CI. $^*P < 0.05$, $^{**}P < 0.01$; ANOVA with Tukey–Kramer HSD test.

F Representative presentation of increased RNA foci in *C9orf72* carriers upon lentiviral-mediated hnRNPA3 knockdown. Scale bar, 10 μm.

G Quantification of the number of RNA foci (fold change). Three cases were analyzed. Single points indicate an average obtained from 29 to 30 cells per case. Color code labels values obtained in fibroblasts derived from the three individual patients. Mean ± SEM. $^{**}P < 0.01$; two-tailed *t*-test.

Source data are available online for this figure.

different monoclonal antibodies, we focused on enhanced formation of RNA foci, which consistently accumulate upon hnRNPA3 knockdown in HeLa cells (see Fig 1F and G). Two independent siRNAs efficiently knocked down hnRNPA3 and lowered hnRNPA3 protein levels in all three fibroblast lines (Fig 5B), where RNA foci composed of the repeat RNA could be detected by *in situ* hybridization (Fig 5C). As a result of lowered hnRNPA3, we observed an approximately two fold increase of cells containing RNA foci (Fig 5D). In addition, hnRNPA3 knockdown significantly increased the number of foci per individual cell (Fig 5E). These findings were independently confirmed using lentiviral-mediated knockdown (Fig 5F and G). Taken together, these results confirm regulation of the GGGGCC repeat RNA by hnRNPA3 on an endogenous level in patient-derived primary cells.

Nuclear hnRNPA3 reduction correlates with poly-GA accumulation in *C9orf72* patients

Enhanced generation of poly-GA deposits and RNA foci in primary neurons and patient's fibroblasts upon hnRNPA3 knockdown prompted us to investigate the link between reduced hnRNPA3 expression and DPR deposition in brains of patients with *C9orf72* repeat extensions. To do so, we performed double immunofluorescence with anti-hnRNPA3 and anti-GA antibodies in hippocampal sections, where hnRNPA3-related pathology was most prominent and abundant DPR pathology was observed [3,4,6]. Two examiners independently analyzed sections from 34 *C9orf72* cases. In *C9orf72* patients, we frequently detected individual neurons with reduced nuclear hnRNPA3 as well as partial co-localization of hnRNPA3 with poly-GA aggregates (Fig 6A and B). When we grouped the cases according to their hnRNPA3 expression levels split at the median, we observed a significant increase in GA deposition in neurons with low hnRNPA3 expression (Fig 6C). Approximately 50% higher levels of poly-GA deposits in cases with low hnRNPA3 levels are comparable to the effect of hnRNPA3 knockdown of RNA foci in patient fibroblasts (Fig 5). This is also in line with the data derived from cultured cells, where lowering of hnRNPA3 leads to higher levels of poly-GA.

Discussion

Reduced hnRNPA3 increases the levels of the G_4C_2 repeat RNA in three independent tissue culture systems. As a consequence, DPR production and deposition is elevated as well. This occurs independent of promotor effects, as two different promotors were used to drive ectopic expression G_4C_2 repeats and controls with an irrelevant reporter protein were included as well. Moreover, in patient-derived fibroblasts, we also observed an accumulation of RNA foci similar to the results in HeLa cells. These findings suggest that binding of hnRNPA3 to the repeat RNA reduces its stability and thus decreases its levels. Binding of hnRNPA3 to the repeat RNA may lead to a reduction of its secondary structure, which could facilitate its degradation. In line with the emerging evidence that *C9orf72* repeat extensions disturb nuclear transport [11–13], these findings may suggest that *C9orf72* repeat-associated toxicity affects nuclear import of hnRNPA3 and thus triggers a vicious cycle, although a direct effect of repeat-mediated toxicity on hnRNPA3 nuclear transport remains to be shown. By reducing nuclear hnRNPA3, the repeat RNA stability may be increased with the consequence of enhanced RNA foci formation and DPR deposition, which in turn may further reduce nuclear transport. Regardless whether accumulation of the repeat RNA or the DPRs are more

Figure 6. Nuclear hnRNPA3 reduction correlates with poly-GA accumulation in patients with *C9orf72* repeat expansions.

A Double immunofluorescence staining with anti-GA (green) and anti-hnRNPA3 (red) antibodies of the granular layer of the dentate gyrus of a control case and three *C9orf72* mutation cases. In C9 mutation cases with low nuclear hnRNPA3 expression (#8 & #1), more poly-GA aggregates were observed as in cases with high nuclear hnRNPA3 (#7). Inserts show examples of co-localization of poly-GA and hnRNPA3 aggregates. Scale bar, 10 μm.

B Granular layer neurons of a *C9orf72* mutation case with (white arrows) or without (orange arrows) nuclear clearance of hnRNPA3. Scale bar, 10 μm.

C Poly-GA aggregates are more frequent in *C9orf72* mutation cases with lower nuclear hnRNPA3 levels than in those cases with higher nuclear hnRNPA3 levels (divided by median of nuclear hnRNPA3 intensities in 34 *C9orf72* mutation cases into two subgroups). Bar graph indicates mean values. Error bars indicate 95% CI. Single points indicate mean from three micrographs per case. Note that the difference in GA positivity between both groups remains significant ($P = 0.0086$) after removal of the highest outlier in the low nuclear A3 group; two-tailed *t*-test.

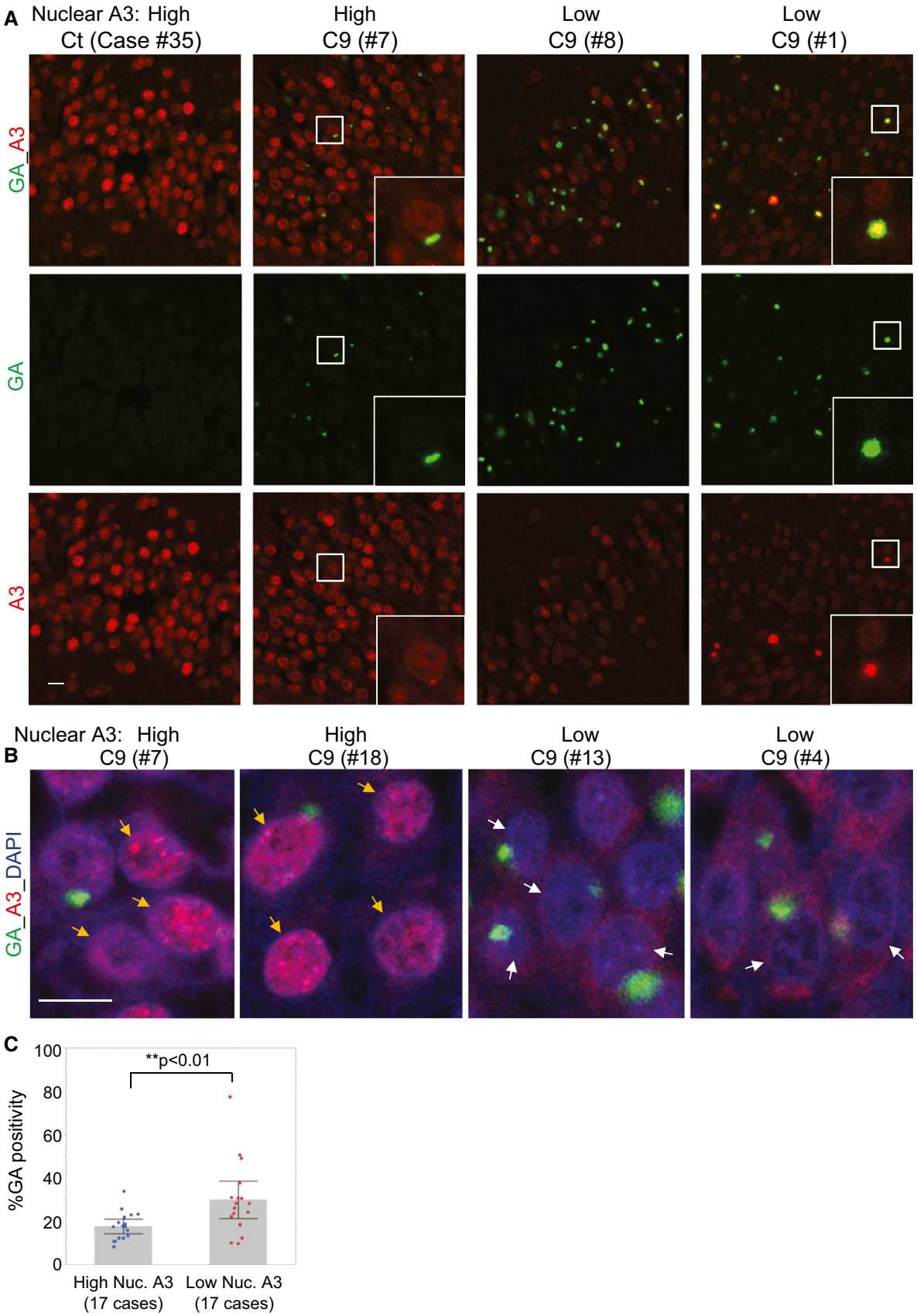

Figure 6.

neurotoxic [7,8,14–20], lowered nuclear hnRNPA3 levels may thus facilitate neurodegeneration.

Materials and Methods

Cell culture

HeLa cells were cultured in DMEM containing 10% FCS and Penicillin/Streptomycin. Rat primary neurons were prepared from embryonic day 18 Sprague Dawley rat embryos as described previously [21].

Patient-derived fibroblasts

We included cell lines from 3 *C9orf72* ALS patients (Fig 5A). All procedures were in accordance with the Helsinki convention and approved by the Ethical Committee of the University of Dresden (EK45022009; EK393122012). Patients were genotyped using EDTA blood in the clinical setting after given written consent according to German legislation independent of any scientific study by a diagnostic human genetic laboratory (CEGAT, Tübingen, Germany or Department of Human Genetics, University of Ulm, Germany) using diagnostic standards.

Skin biopsies were obtained after written informed consent by performing biopsies at the legs of the respective patients. For establishing fibroblast lines from skin biopsies, tissue was manually dissected into pieces of approximately 1 cm^2 in size, collected by centrifugation at 200 *g* for 4 min and digested with trypsin (2.5 mg/ml, Sigma-Aldrich) for 20 min at room temperature. Digested tissue was centrifuged at 200 *g* for 4 min and incubated with DNase (0.04 mg/ml, Sigma-Aldrich) for 10 min at 37°C. Tissue was collected by centrifugation and further disaggregated by incubation with collagenase type II (20 mg/ml, PAA) for 30 min at 37°C. Cells were plated onto tissue culture treated plates in fibroblast media containing DMEM high glucose (Invitrogen), 20% FCS (PAA), 1.1% sodium pyruvate (Invitrogen), 1% penicillin/streptomycin/glutamine (Invitrogen), and 0.4% uridine (50 μg/ml, Sigma-Aldrich). Cells were split using standard trypsination protocols.

Plasmids

The $(G_4C_2)_{80}$ expression vector is based on the previously published cDNA construct [4]. The modified vector expresses 80 GGGGCC repeats under the control of the EF1 promoter including 113 bp of the 5′ flanking region of the human *C9orf72* GGGGCC repeat. The 5′ flanking region contains multiple stop codons in each reading frame and lacks an ATG initiation codon. In addition to the V5/His-tag derived from the vector pEF6-V5/His (Thermo Fisher Scientific), a HA- and a FLAG-tag was introduced in the two remaining reading frames, respectively.

To generate a control vector lacking the G_4C_2 repeats (0rp), repeats were deleted in a two-step PCR protocol and then subcloned into BamHI/XbaI site of the same vector.

The pEF6-pEFGP vector was obtained by exchanging the BamHI/NotI (5′ flanking region and repeat region) fragment of the $(G_4C_2)_{80}$ vector with the EGFP coding sequence including a Kozak sequence and an ATG start codon.

To obtain the high expression repeat constructs $(G_4C_2)_{80}$HIGH(+0), $(G_4C_2)_{80}$HIGH(+1), and $(G_4C_2)_{80}$HIGH(+2) shown in Fig EV2A, the BamHI/XbaI fragment of the $(G_4C_2)_{80}$ vector (including the 5′ flanking region, the repeat region, and a tag) was subcloned into pcDNA4TO myc/His B vector. Frame shift deletions were introduced into a linker sequence located just 5′ of the tag encoding sequence of $(G_4C_2)_{80}$HIGH(+0) plasmid. This generated individual tags for each DPR (e.g., GA has a FLAG-tag in $(G_4C_2)_{80}$HIGH(+0), a HA-tag in $(G_4C_2)_{80}$HIGH(+1), and a myc-tag in $(G_4C_2)_{80}$HIGH(+2)). Repeat length was verified with restriction enzyme digestion/electrophoresis upon each preparation.

To obtain mCherry-fusion constructs introduced in Figs 1C and 2A and D, the mCherry coding sequence was first subcloned into HindIII/KpnI sites of pcDNA5FRT/TO vector (mCh vector). The hnRNPA2 coding sequence was subcloned into KpnI/NotI sites of the mCh vector (mCh-A2 vector). Since the long glycine-rich region of hnRNPA3 is unstable in bacteria, we designed a codon-optimized version of hnRNPA3 in which repetitive and secondary structure-forming sequences were minimized while keeping the primary amino acid sequence intact. The codon-optimized hnRNPA3 was subcloned into KpnI/NotI sites of the mCh vector (mCh-A3 vector). A DNA fragment encoding the hnRNP A3 DxD mutant ($F_{78}xF_{80}$ and $F_{169}xF_{171}$ to $D_{78x}D_{80}$ and $D_{169}xD_{171}$) was synthesized and subcloned into the KpnI/NotI site of the mCh vector (mCh-A3DxD vector). The hnRNPA3ΔM9 mutation was obtained by insertion of a stop codon just before the M9 core region (NYSGQQQ$_{340}$*stop) using PCR mutagenesis (mCh-A3ΔM9 vector). The mCherry-hnRNPA3 fusion constructs are siRNA-resistant since the corresponding nucleotide sequences were altered during codon optimization.

shRNA targeting rat hnRNPA3 (target sequence GATGGTGGATA TAATGGAT) and firefly luciferase (targeting CGTACGCGGAATA CTTCGA) as a control [21] were expressed from the H1 promoter of a lentiviral vector co-expressing tagRFP from human ubiquitin C promoter. To achieve hnRNPA3 knockdown in patient-derived fibroblasts, shRNA targeting human hnRNPA3 (target sequence GATGGTGGATATAATGGAT) and firefly luciferase (targeting CGTA CGCGGAATACTTCGA) as a control were subcloned into a lentiviral vector co-expressing GFP.

siRNA-mediated knockdown and plasmid transfection

The following siRNAs were obtained from Dharmacon: ON-TARGETplus human non-targeting siRNA D-001810-01, hnRNP A1 J-008221-11 CAACUUCGGUCGUGGAGGA, hnRNPA2B1#10 GCUGU UUGUUGGCGGAAUU, hnRNPA3 J-019347-08 ACAAUGAAGGAG GAAAUUU, hnRNPA3 J-019347-06 GGAGGGAACUUUGGAGGUG, hnRNPH1 J-012107-08 UAACAUUGCCGGUGGACUU, J-013245-20 hnRNPH2 GGCAAGUGGUGGCGCUUAU. Ten nanomoles of each siRNA was reverse transfected using RNAiMax (Thermo Fisher Scientific) and OPTI-MEM. After overnight incubation, media were exchanged and 0.5 μg/well (in the case of 24-well plate) of plasmids were transfected with lipofectamine ltx with plus reagent (Thermo Fisher Scientific) with OPTI-MEM. For rescue experiments, 0.4 μg of repeat expressing plasmids and 0.2 μg rescue constructs were co-transfected. Media were exchanged after 4- to 6-h incubation. Cells were harvested 2 days after plasmid transfection unless otherwise indicated.

Antibodies

The following antibodies were used for Western blots (WB) and immunofluorescence (IF): anti-hnRNP A1 clone 4B10 (Sigma-Aldrich) WB 1/8,000, anti-hnRNP A2/B1 clone DP3B3 (Sigma-Aldrich) WB 1/10,000, anti-hnRNP A3ab1 (Sigma-Aldrich, AV41195, lot No. QC10071) WB 1/2,000, IF 1/100 (cultured cells), and 1/150 (human brain sections), anti-hnRNPH (Abcam, ab10374) WB 1/10,000, anti-TDP-43 (Proteintech 10782-2-AP) IF 1/500, anti-p62 (Abcam, ab56416) IF 1/500, anti-FLAG clone M2 (Sigma-Aldrich) WB 1/4,000, anti-DYKDDDDK(FLAG) Tag (Cell Signaling #2368S) WB 1/1,000, IF 1/800, anti-myc clone 9E10 (Santa Cruz) WB 1/1,000, IF 1/100, anti-V5 (Santa Cruz), anti-HA Tag clone 3F10 (Roche) WB 1/1,000, IF 1/100, anti-GFP clone N86/8 (Neuromab) WB 1/3,000, anti-mCherry (Abcam, ab167453) WB 1/20,000, anti-beta-actin (Sigma-Aldrich) WB 1/2,000, anti-Tuj1 IF 1/1,000 (Covance, MRB-435P), anti-NCL antibody (Abcam, ab136649) IF 1/1,000, and anti-GA WB 1/100, IF 1/500 (Mackenzie *et al* [22]).

Filter trap analysis in HeLa cells

Cells cultured in 12-well plates were lysed with 600 μl of lysis buffer (25 mM HEPES pH 7.6, 150 mM NaCl, 3% SDS, 0.5% sodium deoxycholate, 1% Triton X-100) supplemented with protease inhibitor cocktail (Sigma-Aldrich) for 10 min and passed through 27G needle for 10 times. The lysates were further diluted 1:5 or 1:25 with the lysis buffer. Hundred microliters of each sample was filtered through a nitrocellulose membrane (0.45 μm pore). The membrane was subsequently boiled in PBS for 10 min, washed once with TBST, and then blocked in I-Block/PBS/TX100. Levels of each DPR were analyzed with antibodies against all three different tags to exclude different antibody sensitivities. Quantified signals from 3 independent filter trap analyses probed with 3 different tag antibodies (total 9 membranes) are shown as fold expression.

Filter trap analysis of rat primary neuron

Neurons cultured in 12-well plates were lysed with 600 μl Triton buffer (0.1% Triton X-100, 15 nM $MgCl_2$ in PBS, supplemented with DNase and protease inhibitor) on ice. After centrifugation at 17,000 *g* at 4°C for 30 min, pellet was resolved in 200 μl SDS-Tris buffer containing 2% SDS and 100 mM Tris pH 7 for 1 h at room temperature. The lysates were further diluted 1:1 with the SDS-Tris buffer. Hundred microliters of each sample was filtered through a cellulose acetate membrane (0.2 μm pore).

Quantitative reverse transcription (qRT)–PCR

Total RNA was prepared using the RNeasy and Qiashredder kit (Qiagen). RNA preparations were treated with Turbo DNA-free kit (Thermo Fisher Scientific) to minimize residual DNA contamination. Two micrograms of RNA was used for reverse transcription with M-MLV Reverse Transcriptase (Promega) using oligo-(dT) 12–18 primer (Invitrogen). qRT–PCR was performed using the 7500 Fast Real-Time PCR System (Applied Biosystems) with TaqMan technology. Primers and probes were designed (IDT) for 3′ TAG region of repeat constructs (repeat TAG primer). Primer 1: TCT CAA ACT GGG ATG CGT AC, Primer 2: GTA GTC AAG CGT AGT CTG GG, Probe/56-FAM/TG CAG ATA T/Zen/C CAG CAC AGT GGC G/3IABkFQ/. For EGFP, Primer 1: GCACAAGCTGGAGT ACAACTA, Primer 2: TGTTGTGGCGGATCTTGAA, Probe/56-FAM/AGCAGAAGA/ZEN/ACGGCATCAAGGTGA/3IABkFQ/. A primer/probe set for Human GAPDH, 4326317E (Applied Biosystems) was used as endogenous control. Each sample was paired with no reverse transcription controls showing < 1/2^10 (ΔCT > 10) signal when compared to reverse transcribed samples, thus excluding contamination of plasmid DNA-derived signal. Each biological sample was analyzed in duplicate or triplicate. Signals of repeat constructs derived cDNA were normalized to GAPDH cDNA according to the $\Delta\Delta C_T$ method.

In situ hybridization

In situ hybridization was performed as previously described [23,24] with slight modifications. 2% paraformaldehyde fixed and perforated cells on glass coverslips were rinsed twice with SSC and then incubated in prehybridization solution (40% formamide (Life Technologies, 15515-026)/2× SSC, 2.5% BSA) at 55°C for 30 min. Cells were then incubated with hybridization solution (40% formamide, 2× SSC, 0.8 mg/ml tRNA (Roche), 0.8 mg/ml single strand salmon sperm DNA (Sigma-Aldrich, D7656), 0.16% BSA, 8% Dextran sulfate (Sigma-Aldrich), 1.6 mM Ribonucleoside vanadyl complex (New England Biolabs, S1402S), 5 mM EDTA, 10 μg/μl 5′ Cy3-labbeled 2′-O-methyl-(CCCCGG)x4 probe (IDT [25])) at 55°C. The following day, cells were sequentially washed in 40% formamide/0.5× SSC for 3 times 30 min each at 55°C and then with 0.5× SSC 3 times 10 min each at room temperature. After a brief rinse with PBS, nuclei were counterstained with 0.5 μg/ml of DAPI for 20 min and then washed with PBS for 3 times 3 min each. Glass coverslips were mounted using Prolong Gold antifade (Life Technologies) and analyzed with LSM710 confocal microscopy with ZEN2011 software (Zeiss).

Human brain samples

All cases provided by the Neurobiobank Munich, Ludwig-Maximilians-University (LMU) Munich, and the University of British Columbia were collected and distributed according to the guidelines of the local ethical committee. Brain autopsy was performed on the basis of informed consent. For further details, see Table EV1.

Quantitative immunofluorescence in human brain sections

Human hippocampal brain sections from 34 cases with *C9orf72* repeats and 5 control cases were stained as described previously [3,4,6] using anti-GA, anti-hnRNPA3 antibodies, and DAPI. Three fluorescent images of the dentate gyrus were obtained from each case using LSM710 (Zeiss) microscope with a 63× oil immersion objective. Raw data tif files of each channel were exported from czi files using Zen2011 software. Quantification was performed using ImageJ software. Binary images from DAPI staining were used for the nuclear regions. Vascular structures were manually excluded from the analysis. Cell numbers of each image were counted.

Nuclear hnRNPA3 was defined as hnRNPA3 signal overlapping with DAPI staining. The hnRNPA3 signal from surrounding tissue outside of cell bodies was regarded as background. After subtraction of background, nuclear hnRNPA3 intensities of about 80–180 granular layer cells/case were quantified in 34 *C9orf72* cases. Median nuclear hnRNPA3 intensity (arbitrary unit) of these cells per micrograph was defined as the nuclear hnRNPA3 level of each image. An average of the nuclear hnRNPA3 levels of 3 micrographs from a *C9orf72* case was regarded as the nuclear hnRNPA3 level of the case. The 34 *C9orf72* mutation cases were then separated at the median of the nuclear hnRNPA3 levels (see also Table EV1) of the 34 cases (cutoff = 4.93) into two groups expressing low or high hnRNPA3 levels (n = 17, 17; mean nuclear hnRNPA3 level ± SEM: 10.28 ± 2.220 (High), 3.353 ± 0.2000 (Low)). There is no statistically significant difference between the two groups in gender (n of male: n of female = 11:6 (A3 High), 11:6 (A3 Low), two-sided chi-square test, $P = 1.000$), age of onset (mean ± SEM = 57.0714 ± 1.7082 (A3 High), 55.8824 ± 1.5502 (A3 Low), two-sided t-test, $t = -0.51548$, df = 29, $P = 0.6101$), age of death (mean ± SEM = 62.6250 ± 1.8835 (A3 High), 61.6471 ± 1.8273 (A3 Low), two-sided t-test, $t = -0.37266$, df = 31, $P = 0.7119$), disease duration in years (mean ± SEM = 4.33571 ± 1.2647 (A3 High), 5.73529 ± 1.1477 (A3 Low), two-sided t-test, $t = 0.819517$, df = 29, $P = 0.4192$). Postmortem delays were longer in the high A3 group (mean ± SEM = 71.2143 ± 9.0220 h (A3 High), 31.8667 ± 8.7161 h (A3 Low), two-sided t-test, $t = -3.13661$, df = 27, $P = 0.0041$). However, cases #3 and #5 had an exceptionally long postmortem delay of, respectively, 131–134 h or approximately 190 h. The numbers of poly-GA aggregates in the same field were counted. The number of poly-GA inclusions/number of cells ×100 was displayed as % poly-GA positivity of respective cases. Scale bar = 10 μm. Quantification is shown as a bar graph. Single dots represent an average data obtained from three microscopic images from a case.

Statistics

Statistical analysis was performed using Prism 5 for Mac OS X (GraphPad Software, Inc) or JMP Pro 12.2.0 software.

Expanded View for this article is available online.

Acknowledgements

This work was supported by the European Research Council under the European Union's Seventh Framework Program (FP7/2007-2013)/ERC Grant Agreement No. 617198 (DPR-MODELS to D.E.), the Deutsche Forschungsgemeinschaft (German Research Foundation) within the framework of the Munich Cluster for System Neurology (EXC 1010 SyNergy), and the MetLife Foundation award (CH). A.H. and C.H. are supported by the Helmholtz Virtual Institute "RNA dysmetabolism in ALS and FTD (VI-510)" and the NOMIS Foundation. We thank Ms. Iryna Pigur for generating brain sections and Drs. Anja Capell and Gernot Kleinberger for critically reading our manuscript.

Author contributions

CH and KM conceived the research concept. CH coordinated the study. KM performed and analyzed most experiments except the following; KM and YN analyzed human brain tissue. YN and QZ performed the experiments in primary fibroblasts. The experiments using rat primary neuron were designed and performed by QZ, DO, and DE. DE provided materials and valuable conceptual advice. AH and FH established fibroblast lines from three *C9orf72* carriers. FK and BN provided important biophysical insights. IRM and TA collected, diagnosed, and provided human brain tissue and supervised neuropathological analyses; the German Consortium for Frontotemporal Lobar Degeneration and the Bavarian Brain Banking Alliance identified patients with *C9orf72* mutations and provided brains; CH wrote the manuscript together with KM and input from all authors.

Conflict of interest

The authors declare that they have no conflict of interest.

References

1. Ash PE, Bieniek KF, Gendron TF, Caulfield T, Lin WL, Dejesus-Hernandez M, van Blitterswijk MM, Jansen-West K, Paul JW 3rd, Rademakers R *et al* (2013) Unconventional translation of C9ORF72 GGGGCC expansion generates insoluble polypeptides specific to c9FTD/ALS. *Neuron* 77: 639 – 646
2. Gendron TF, Bieniek KF, Zhang YJ, Jansen-West K, Ash PE, Caulfield T, Daughrity L, Dunmore JH, Castanedes-Casey M, Chew J *et al* (2013) Antisense transcripts of the expanded C9ORF72 hexanucleotide repeat form nuclear RNA foci and undergo repeat-associated non-ATG translation in c9FTD/ALS. *Acta Neuropathol* 126: 829 – 844
3. Mori K, Arzberger T, Grasser FA, Gijselinck I, May S, Rentzsch K, Weng SM, Schludi MH, van der Zee J, Cruts M *et al* (2013) Bidirectional transcripts of the expanded C9orf72 hexanucleotide repeat are translated into aggregating dipeptide repeat proteins. *Acta Neuropathol* 126: 881 – 893
4. Mori K, Weng SM, Arzberger T, May S, Rentzsch K, Kremmer E, Schmid B, Kretzschmar HA, Cruts M, Van Broeckhoven C *et al* (2013) The C9orf72 GGGGCC repeat is translated into aggregating dipeptide-repeat proteins in FTLD/ALS. *Science* 339: 1335 – 1338
5. Zu T, Liu Y, Banez-Coronel M, Reid T, Pletnikova O, Lewis J, Miller TM, Harms MB, Falchook AE, Subramony SH *et al* (2013) RAN proteins and RNA foci from antisense transcripts in C9ORF72 ALS and frontotemporal dementia. *Proc Natl Acad Sci U S A* 110: E4968 – E4977
6. Mori K, Lammich S, Mackenzie IR, Forne I, Zilow S, Kretzschmar H, Edbauer D, Janssens J, Kleinberger G, Cruts M *et al* (2013) hnRNP A3 binds to GGGGCC repeats and is a constituent of p62-positive/TDP43-negative inclusions in the hippocampus of patients with C9orf72 mutations. *Acta Neuropathol* 125: 413 – 423
7. Donnelly CJ, Zhang PW, Pham JT, Heusler AR, Mistry NA, Vidensky S, Daley EL, Poth EM, Hoover B, Fines DM *et al* (2013) RNA Toxicity from the ALS/FTD C9ORF72 Expansion Is Mitigated by Antisense Intervention. *Neuron* 80: 415 – 428
8. Lee YB, Chen HJ, Peres JN, Gomez-Deza J, Attig J, Stalekar M, Troakes C, Nishimura AL, Scotter EL, Vance C *et al* (2013) Hexanucleotide repeats in ALS/FTD form length-dependent RNA foci, sequester RNA binding proteins, and are neurotoxic. *Cell Rep* 5: 1178 – 1186
9. Kim HJ, Kim NC, Wang YD, Scarborough EA, Moore J, Diaz Z, MacLea KS, Freibaum B, Li S, Molliex A *et al* (2013) Mutations in prion-like domains in hnRNPA2B1 and hnRNPA1 cause multisystem proteinopathy and ALS. *Nature* 495: 467 – 473
10. Mayeda A, Munroe SH, Caceres JF, Krainer AR (1994) Function of conserved domains of hnRNP A1 and other hnRNP A/B proteins. *EMBO J* 13: 5483 – 5495

11. Zhang K, Donnelly CJ, Haeusler AR, Grima JC, Machamer JB, Steinwald P, Daley EL, Miller SJ, Cunningham KM, Vidensky S *et al* (2015) The C9orf72 repeat expansion disrupts nucleocytoplasmic transport. *Nature* 525: 56 – 61
12. Freibaum BD, Lu Y, Lopez-Gonzalez R, Kim NC, Almeida S, Lee KH, Badders N, Valentine M, Miller BL, Wong PC *et al* (2015) GGGGCC repeat expansion in C9orf72 compromises nucleocytoplasmic transport. *Nature* 525: 129 – 133
13. Jovicic A, Mertens J, Boeynaems S, Bogaert E, Chai N, Yamada SB, Paul JW 3rd, Sun S, Herdy JR, Bieri G *et al* (2015) Modifiers of C9orf72 dipeptide repeat toxicity connect nucleocytoplasmic transport defects to FTD/ALS. *Nat Neurosci* 18: 1226 – 1229
14. Haeusler AR, Donnelly CJ, Periz G, Simko EA, Shaw PG, Kim MS, Maragakis NJ, Troncoso JC, Pandey A, Sattler R *et al* (2014) C9orf72 nucleotide repeat structures initiate molecular cascades of disease. *Nature* 507: 195 – 200
15. Mizielinska S, Gronke S, Niccoli T, Ridler CE, Clayton EL, Devoy A, Moens T, Norona FE, Woollacott IO, Pietrzyk J *et al* (2014) C9orf72 repeat expansions cause neurodegeneration in Drosophila through arginine-rich proteins. *Science* 345: 1192 – 1194
16. Kwon I, Xiang S, Kato M, Wu L, Theodoropoulos P, Wang T, Kim J, Yun J, Xie Y, McKnight SL (2014) Poly-dipeptides encoded by the C9orf72 repeats bind nucleoli, impede RNA biogenesis, and kill cells. *Science* 345: 1139 – 1145
17. May S, Hornburg D, Schludi MH, Arzberger T, Rentzsch K, Schwenk BM, Grasser FA, Mori K, Kremmer E, Banzhaf-Strathmann J *et al* (2014) C9orf72 FTLD/ALS-associated Gly-Ala dipeptide repeat proteins cause neuronal toxicity and Unc119 sequestration. *Acta Neuropathol* 128: 485 – 503
18. Chew J, Gendron TF, Prudencio M, Sasaguri H, Zhang YJ, Castanedes-Casey M, Lee CW, Jansen-West K, Kurti A, Murray ME *et al* (2015) C9ORF72 repeat expansions in mice cause TDP-43 pathology, neuronal loss, and behavioral deficits. *Science* 348: 1151 – 1154
19. Wen X, Tan W, Westergard T, Krishnamurthy K, Markandaiah SS, Shi Y, Lin S, Shneider NA, Monaghan J, Pandey UB *et al* (2014) Antisense proline-arginine RAN dipeptides linked to C9ORF72-ALS/FTD form toxic nuclear aggregates that initiate in vitro and in vivo neuronal death. *Neuron* 84: 1213 – 1225
20. Tran H, Almeida S, Moore J, Gendron TF, Chalasani U, Lu Y, Du X, Nickerson JA, Petrucelli L, Weng Z *et al* (2015) Differential Toxicity of Nuclear RNA Foci versus Dipeptide Repeat Proteins in a Drosophila Model of C9ORF72 FTD/ALS. *Neuron* 87: 1207 – 1214
21. Orozco D, Tahirovic S, Rentzsch K, Schwenk BM, Haass C, Edbauer D (2012) Loss of fused in sarcoma (FUS) promotes pathological Tau splicing. *EMBO Rep* 13: 759 – 764
22. Mackenzie IR, Arzberger T, Kremmer E, Troost D, Lorenzl S, Mori K, Weng SM, Haass C, Kretzschmar HA, Edbauer D *et al* (2013) Dipeptide repeat protein pathology in C9ORF72 mutation cases: clinico-pathological correlations. *Acta Neuropathol* 126: 859 – 879
23. Mizielinska S, Lashley T, Norona FE, Clayton EL, Ridler CE, Fratta P, Isaacs AM (2013) C9orf72 frontotemporal lobar degeneration is characterised by frequent neuronal sense and antisense RNA foci. *Acta Neuropathol* 126: 845 – 857
24. Schludi MH, May S, Grasser FA, Rentzsch K, Kremmer E, Kupper C, Klopstock T, German Consortium for Frontotemporal Lobar Degeneration, Bavarian Brain Banking Alliance, Arzberger T *et al* (2015) Distribution of dipeptide repeat proteins in cellular models and C9orf72 mutation cases suggests link to transcriptional silencing. *Acta Neuropathol* 130: 537 – 555
25. DeJesus-Hernandez M, Mackenzie IR, Boeve BF, Boxer AL, Baker M, Rutherford NJ, Nicholson AM, Finch NA, Flynn H, Adamson J *et al* (2011) Expanded GGGGCC hexanucleotide repeat in noncoding region of C9ORF72 causes chromosome 9p-linked FTD and ALS. *Neuron* 72: 245 – 256